Computing contact angles for oil–water–rock systems via thermodynamic integration

🆔 Rohan Patel, 🆔 Ravi Kumar Reddy Addula, Majeed Shaik, et al.

COLLECTIONS

Paper published as part of the special topic on Fluids Meet Solids
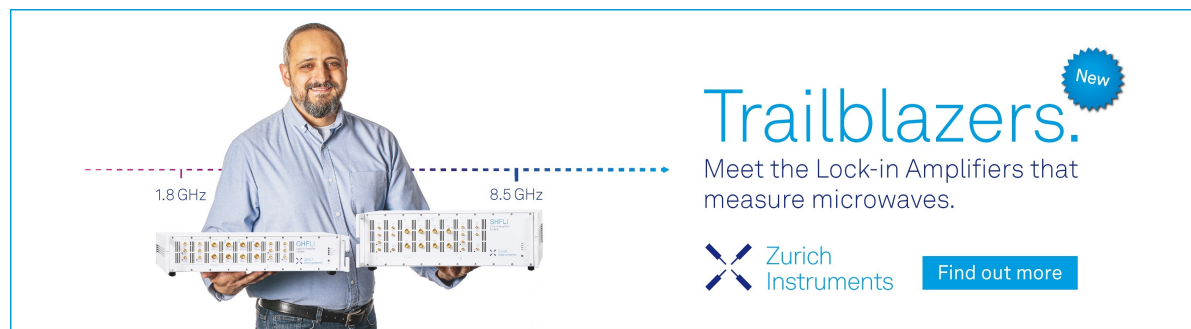
🌐 **View Online**   ⬆ **Export Citation**   🔴 **CrossMark**

ARTICLES YOU MAY BE INTERESTED IN

Kirkwood–Buff integrals: From fluctuations in finite volumes to the thermodynamic limit
The Journal of Chemical Physics **157**, 130901 (2022); https://doi.org/10.1063/5.0106162

A unified framework of transformations based on the Jordan–Wigner transformation
The Journal of Chemical Physics **157**, 134104 (2022); https://doi.org/10.1063/5.0107546

Alternating one-phase and two-phase crystallization mechanisms in octahedral patchy colloids
The Journal of Chemical Physics **157**, 134501 (2022); https://doi.org/10.1063/5.0101529

Computing contact angles for oil–water–rock systems via thermodynamic integration

Rohan Patel,[1] (iD) Ravi Kumar Reddy Addula,[2] (iD) Majeed Shaik,[3] and Sudeep N. Punnathanam[1,a) (iD)

AFFILIATIONS

[1] Department of Chemical Engineering, Indian Institute of Science, Bangalore 560012, India
[2] Chemical and Biomolecular Engineering, University of Illinois at Urbana-Champaign, Urbana, Illinois 61801, USA
[3] Shell India Markets Pvt. Ltd., Bangalore 562149, India

Note: This paper is part of the JCP Special Topic on Fluids Meets Solids.
[a)]Author to whom correspondence should be addressed: sudeep@iisc.ac.in

ABSTRACT

Wettability of rock surfaces with respect to oil and water, which is characterized by the contact angle, is an important factor that determines the efficacy of enhanced oil recovery operations. Experimental determination of contact angles for oil–water–rock systems is expensive and time-consuming due to the extremely long times needed for the establishment of adsorption equilibrium at the liquid–solid interface. Hence, molecular simulations form an attractive tool for computing contact angles. In this work, we use the cleaving wall technique that was developed previously in our group [R. K. R. Addula and S. N. Punnathanam, J. Chem. Phys. **153**, 154504 (2020)] to compute solid–liquid interfacial free energy, which is then combined with Young's equation to compute the oil–water contact angle on silica surfaces. The silica surface is modeled with the INTERFACE force field that has been developed to accurately reproduce experimental data. We have considered three different surface chemistries of silica, namely, Q_2, Q_3, and Q_4, in this study. Our calculations reveal that while the Q_2 and Q_3 surfaces are completely wetted by water, the Q_4 surface is partially non-wetted by water. All the simulations needed for this calculation can be performed using the Large-scale Atomic/Molecular Massively Parallel Simulator (LAMMPS) molecular package. This should facilitate wider adoption of the Young's equation route to compute contact angles for systems comprised of complex molecules.

Published under an exclusive license by AIP Publishing. https://doi.org/10.1063/5.0101013

I. INTRODUCTION

Energy consumption is the fulcrum of modern societies and increasing growth in the world economy is accompanied by a proportionate increase in the world energy consumption. The many sources of energy include conventional ones—such as fossil fuels, hydel power, and nuclear power—and nonconventional ones—such as solar, wind, and geothermal. Although the share of nonconventional sources is increasing, it is expected that the conventional energy sources will remain dominant for the foreseeable future. Among the conventional sources, energy from crude oil constitutes about 31% of world demand.[1,2] Hence, to meet increasing energy demands, it is essential to develop technologies to improve the recoverability of oil from reservoirs. Among these is the enhanced oil recovery (EOR) technology, used after ~50%–55% of original oil in place (OOIP) is recovered[2–6] and the pressure inside the reservoir

is no longer high enough to sustain production. The EOR stage consists of injecting the reservoir with fluids or other agents that modify the physical and/or chemical properties of the reservoir, such as the reservoir rock wettability, and increase the recovery factor and the lifetime of the oil fields.

Crude oil has naturally occurring surface-active molecules that cause them to be preferentially oil wet[7] and cover the rock surfaces of the reservoir. For enhanced oil recovery to be effective, the injected fluid needs to wet the rock surface preferentially compared to the oil phase. The angle, θ, formed by a drop of water on the rock surface while immersed inside the oil phase characterizes the wettability of the rock surface. It is called the equilibrium contact angle and is a measure of the balance of forces caused by the interfacial tensions between the three interfaces. When $\theta < 0°$, the surface is water wet, and when $\theta > 180°$, the surface is oil wet. The value of θ is measured experimentally by the sessile drop method. In this method, a

drop of liquid is placed on the solid surface, an image of the droplet is captured in a camera, and the contact angle is measured from the geometry of the droplet. Experimental measurements of contact angles are very challenging. When contact angles are measured in a laboratory, it is important that all the interfaces are in adsorption equilibrium. However, studies have shown that the time needed to reach equilibrium for an oil–water–rock system can approach several hundreds of hours, making such measurements very costly.[7]

These difficulties motivate the use of molecular simulations to estimate contact angles. There are two main approaches toward computing the contact angle using molecular simulations. One is the direct approach, in which a droplet is placed on the surface and the contact angle is directly measured from the geometry of the droplet. This method essentially mimics the sessile drop technique used in experiments. Since the method is rather simple to implement, it is quite popular and widely used to estimate contact angles.[8–13] The earliest application of this method includes estimation of contact angles of water droplets on various surfaces. Examples of such studies include estimation of contact angles on kaolinite,[14] alumina,[15] graphene,[16] and graphene oxide.[17] In later studies, the direct estimation method has extended to compute contact angles of water immersed in a second fluid, usually supercritical CO_2 or model oil. Javanbakht et al.[8] computed the contact angles in the CO_2–water–quartz system and studied the impact of carbonic acid on interfacial properties. Similarly, Silvestri et al.[10] applied the direct contact angle method to CO_2–water–calcite system and Sun and Bourg[12] computed contact angles on CO_2–water–silica system. The simulations of Le, Striolo, and Cole[13] showed that the presence of NaCl in water increased the affinity of supercritical CO_2 to calcite surface. However, the computed values were strongly dependent on the type of force field being used. Jiménez-Ángeles and Firoozabadi[9] computed contact angles in model oil–water–mica system and found that addition of salt makes the surface less oil wet due to ionic adsorption. Zhao, Yao, and Wen[18] investigated the salinity effects on the contact angle of n-decane immersed in water on a calcite surface. They found that increasing salinity led to a slight enhancement of surface hydrophilicity. Direct estimation of contact angles, however, comes with important caveats.[19,20] The main criticism of the direct estimation method is the use of nanometer-sized droplets due to computational limitations, whereas experimental measurements are conducted on macroscopic droplets. This leads to significant finite-size effects on the estimated value of the contact angle. Moreover, at such small sizes, the line tension along the three phase contact line also plays a significant role in determining the shape of the droplet. This situation is partly addressed by simulating a cylindrical droplet under periodic boundary conditions (PBCs) and, thus, eliminating the curvature of the three phase contact line. There is also considerable ambiguity in determining the precise location of the interface, which is important to determine the shape of the droplet. Another potential limitation arises when the fluid phases contain components in small concentrations. In EOR, one is rarely interested in the contact angle of pure water. The goal is to design additives for water that can preferentially wet the rock surface. These additives are typically present in small concentrations and would adsorb on to the solid surface. Hence, we anticipate the need to simulate very large droplets to estimate the contact angle for such systems.

An alternative to the direct estimation of the contact angle is to use Young's equation, i.e.,

$$\cos \theta = \frac{\gamma^{(so)} - \gamma^{(sw)}}{\gamma^{(ow)}}, \quad (1)$$

where γ is the interfacial free energy between any two given phases. The superscripts s, o, and w represent the rock, oil, and water, respectively. This route of contact angle estimation does not suffer from the limitations arising from the finite size of droplets. The estimated contact angle can also be directly compared to the values measured in experiments since Young's equation is valid at the macroscopic level. The interfacial free energy between two fluids can be computed from molecular simulations in a straightforward manner through integration of the anisotropy of the pressure tensor[21] across the interface, i.e.,

$$\gamma^{(ow)} = \frac{1}{2} \int_{-\infty}^{\infty} \left(P_{zz} - \frac{P_{xx} + P_{yy}}{2} \right) dz, \quad (2)$$

where the interface is perpendicular to the z axis, and P_{xx}, P_{yy}, and P_{zz} are the values of components of the pressure tensor at various values of z. However, this technique cannot be used to compute the interfacial free energy between a solid and a fluid due to the presence of internal stresses inside the solid phase. Instead, a host of techniques have been developed to compute the solid–fluid interfacial free energies.[22–30] In all of these techniques, a solid–fluid interface is created starting from a reference system in a reversible manner. The change in free energy during this process is computed, which, in turn, is used to estimate the interfacial free energy. The most common approach is to reversibly cleave the solid and liquid phases and then bring them together to create the solid–fluid interface. We use the term "cleaving wall" to describe these classes of methods. Examples of studies that use this approach include those by Broughton and Gilmer,[22] Davidchack and Laird,[23] Leroy, dos Santos, and Müller-Plathe,[26] Benjamin and Horbach,[27] Qi, Zhou, and Fichthorn.[29] The methods developed by groups of Errington[25] and Müller-Plathe[26] estimate the contact angle by exploiting the fact that one needs to only compute the relative difference between the two solid–fluid interfacial free energies in Young's equation. Errington's approach uses Monte Carlo simulations in the grand canonical ensemble combined with transition matrix Monte Carlo to compute the spreading coefficient of one liquid on a surface immersed in the other liquid. The grand canonical transition matrix Monte Carlo computes the probability distribution of particle numbers in the simulation box. From this information, one can directly compute the extensive spreading coefficient. The difference in the spreading coefficients is equal to the difference in the interfacial free energy. This method has been used to compute interfacial properties of the oil–water–silica system.[31,32] The approach developed by Müller-Plathe,[26] called the phantom wall method, uses thermodynamic integration to compute the solid–liquid interfacial free energy relative to a bare solid surface. Published studies that have used the phantom wall method include computation of contact angles in CO_2–water–silica,[19] hexane–decanoic acid–alumina,[33] and water–hydroxylated silica[34] systems.

In spite of its obvious advantages, the Young's equation route is yet to be widely adopted due to difficulties in applying it to systems

involving complex molecules. The main limitation of the method of Errington is the use of grand canonical ensemble for simulations. This requires Monte Carlo moves that insert/delete molecules to/from the system. This can get problematic for dense systems such as the oil–water–rock system. Although the authors have not given details of the computational time required, we anticipate extremely long simulations to get accurate statistics for probability distribution. In addition, unlike molecular dynamics, the Monte Carlo simulation cannot be parallelized, which leads to extremely long times for the computation. To overcome these challenges, Errington and co-workers are developing methods to compute the spreading coefficient in the isothermal–isobaric[35] and canonical[36] ensembles. These remain a work in progress and are yet to be applied to complex systems. All previous calculations using the cleaving wall techniques required specific strategies to account for the periodic boundary conditions (PBCs) in the solid and liquid phases and to avoid hysteresis along the thermodynamic integration path.[27,29] They were implemented using specialized in-house codes, whose application to systems involving complex molecules is not trivial. As a result, the cleaving wall technique has been applied to relatively simple systems, such as metals,[37] simple atomistic solids,[23,27,38,39] and water.[40,41] The implementation of the phantom wall method by Jiang, Müller-Plathe, and Panagiotopoulos[19] required the authors to make in-house modifications to the Large-scale Atomic/Molecular Massively Parallel Simulator (LAMMPS)[42] molecular dynamics package.

Popular molecular dynamics packages, such as LAMMPS,[42] GROningen MAchine for Chemical Simulations (GROMACS),[43] and Nanoscale Molecular Dynamics (NAMD),[44] have the ability to handle complex molecules described by fully atomistic models. Simulation techniques that can be implemented in such packages can facilitate their adoption by the wider scientific community. To facilitate widespread use of the Young's equation route to compute contact angles by the scientific community, developing techniques that can handle using these molecular dynamics packages can have a significant impact. Toward this objective, we had developed a variation of the cleaving wall method[30] for computing the solid–fluid interfacial free energies. We could compute the contact angle in a system where the fluid and the solid phases were comprised of Lennard-Jones particles. We

also demonstrated the ability of our implementation to handle complex molecules by computing the solid–fluid interfacial free energies between a crystal facet of molecular solids and various solvents. All the simulations needed to estimate the interfacial free energies and contact angles could be performed using the LAMMPS molecular dynamics package without any in-house modification. In this work, we apply the same technique to compute the contact angles formed by a water droplet on a silica surface with the whole systems immersed in an oil phase. The computations are performed for three different types of silica surfaces with varying degrees of hydrophobicity. We demonstrate the ability of our technique to capture the effect of surface chemistries on the contact angle wherever detailed atomistic models of the solid surfaces are available. The choice of the system, i.e., oil–water–rock, is motivated by its economic importance. Since experimental results of the contact angle are currently not available, we also estimate the contact angle through brute force simulations of a water droplet on the silica surfaces and compare the results from the two approaches.

II. CLEAVING WALL METHOD

According to the cleaving wall method,[30] the solid–liquid interface is created reversibly in three steps. In the first step, the liquid is cleaved using a cleaving potential to create space for inserting the solid slab. In the second step, the solid slab is inserted into the cleaved space, and in the third step, the cleaving potential is removed, resulting in the formation of the solid–liquid interface. All the simulations are carried out in the isothermal–isobaric ensemble with volume changes allowed only in the direction perpendicular to the interface, i.e., the solid–liquid interfacial area was kept constant. A schematic representation of the steps involved is shown in Fig. 1. The solid–fluid interfacial free energy, γ, can then be computed as follows:

$$\gamma = \frac{\Delta G_1 + \Delta G_2 + \Delta G_3 + (F^{*(\text{slab})} - F^{*(\text{s})}) - PV^{(\text{s})}}{A}. \quad (3)$$

In this equation, ΔG_1, ΔG_2, and ΔG_3 are the changes in the Gibbs free energy of the system during the three steps mentioned above. The terms $F^{*(\text{slab})}$ and $F^{*(\text{s})}$ are the Helmholtz free energy of the solid
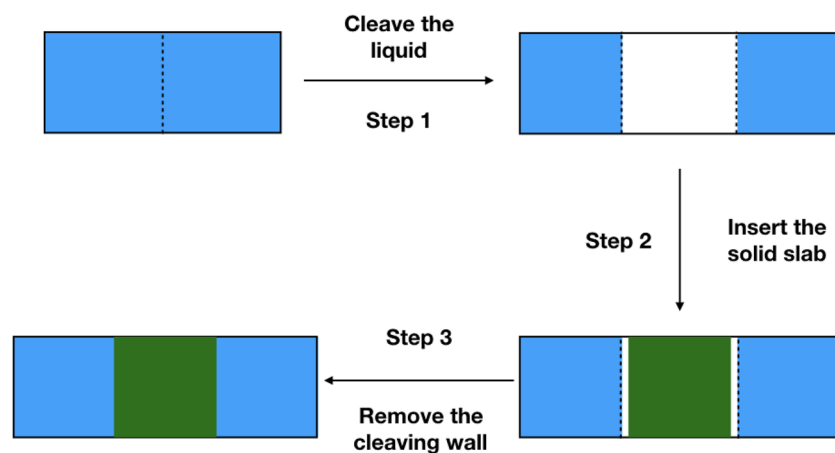

FIG. 1. Stepwise illustration of the cleaving wall method. The blue color indicates the liquid phase and the green color indicates the solid phase.

slab and the bulk solid, respectively. The asterisk indicates that the center of mass is kept constant.[30] The other terms in the equation are the volume of the bulk solid phase, $V^{(s)}$, pressure of the system, P, and the interfacial area, A. The derivation of Eq. (3) is given in Ref. 30. Since we are only interested in the relative interfacial free energies, the free energies of the solid phases get canceled and we only need to compute the free energy changes in the three steps mentioned above. Thus, the difference in the interfacial free energies for the oil–water–rock system can be computed as follows:

$$\gamma^{(so)} - \gamma^{(sw)} = \frac{1}{A}\left\{\left(\Delta G_1^{(o)} + \Delta G_2^{(o)} + \Delta G_3^{(o)}\right) - \left(\Delta G_1^{(w)} + \Delta G_2^{(w)} + \Delta G_3^{(w)}\right)\right\}, \quad (4)$$

where the superscripts (o) and (w) represent the oil and water phase, respectively.

The values of ΔG_1 and ΔG_3 are computed via thermodynamic integration. This is done by performing a series of simulations where a cleaving wall potential, U_w, is modulated by a parameter λ. The value of ΔG_1 can then be computed as follows:[30]

$$\Delta G_1 = -k_B T \, \ln\langle e^{-\beta U_w(\lambda_{min})}\rangle + \int_{\lambda_{min}}^{\lambda_{max}}\left\langle\frac{\partial U_w}{\partial \lambda}\right\rangle d\lambda. \quad (5)$$

In the above equation, the averaging in the first term is over a simulation of pure liquid and the averaging for the terms in the integral is over a system of liquid plus cleaving wall at various values of λ. Similarly, the value of ΔG_3 is computed as[30]

$$\Delta G_3 = k_B T \, \ln\langle e^{-\beta U_w(\lambda_{min})}\rangle - \int_{\lambda_{min}}^{\lambda_{max}}\left\langle\frac{\partial U_w}{\partial \lambda}\right\rangle d\lambda. \quad (6)$$

Here, the averaging in the first term is over a simulation of liquid plus silica and the averaging for the terms in the integral is over a system of liquid, silica, and the cleaving wall at various values of λ. The value of ΔG_2 is computed via thermodynamic perturbation method as follows:[30]

$$\Delta G_2 = -k_B T \, \ln\langle e^{-\beta U_{sf}}\rangle, \quad (7)$$

where U_{sf} is the interaction of the solid slab with the surrounding liquid. The averaging is done over various configurations of the solid and the liquid phases. During this simulation, the solid and the liquid phases do not interact with each other.

A. Differences with phantom wall method

The above strategy of computing the contact angle by only computing the difference in the solid–liquid interfacial free energy is similar to the one used by Leroy, dos Santos, and Müller-Plathe.[26] There are, however, significant differences in the implementation of the strategy between the two methods. The main challenge in both the methods is to maintain a reversible path during the creation of the solid–liquid interface. If not handled properly, this can lead to hysteresis in the path, leading to non-applicability of the thermodynamic integration technique. One of the situations where such problems can arise is when there is strong attraction between the

solid and the liquid. This attraction leads to the formation of layers in the liquid near the interface. In both the methods, when the liquid is separated from the solid, the reduction in the attractive interactions between the liquid and the solid can lead to abrupt change in the structure of the liquid such as occurrence of a drying transition. The phantom wall method overcomes this problem by scaling down the attractive interactions between the solid and liquid before separating the liquid from the interface. In our cleaving wall method, we include an attractive term between the cleaving wall atoms and the liquid atoms. This attractive interaction maintains the structure of the liquid phase near the interface even after the liquid has been separated from the solid slab. Thus, when the solid slab is inserted into the cleaved region during the calculation of ΔG_2, there is minimal change in the liquid structure.

III. MOLECULAR MODELS

Crude oil is mainly trapped in sedimentary rocks due to their porosity. Among the various kinds of rocks, those made of sandstone are most abundant. In this work, we use silica as the model for studying reservoirs primarily made up of sandstone. Depending upon the formation conditions such as temperature, pressure, and pH, silica can exist in many crystalline polymorphs as well as have different surface chemistries. We have studied three different silica surfaces, namely, Q_2, Q_3, and Q_4. The three surfaces differ on the number density of terminal silanol groups. The Q_2 surface has two silanol groups per silicon atom and an area density of 9.4 per nm^2, the Q_3 surface has one silanol group per silicon atom and an area density of 4.7 per nm^2, and the Q_4 surface has zero silanol groups on the surface. Thus, among the three, Q_2 is the most hydrophilic and Q_4 is the most hydrophobic. The interactions of the silica with the fluid phases are modeled using the INTERFACE[45] force field. The INTERFACE force field has been parameterized to resolve numerous shortcomings of prior silica force fields and to reduce uncertainties in computed interfacial properties relative to experiment from several 100% to less than 5%. The Q_2 surface was prepared by cleaving the (100) plane of α-quartz and attaching two OH groups to each exposed silicon atom. A supercell consisting of $7 \times 4 \times 3$ unit cells of quartz was used to prepare the Q_2 surface. The prepared Q_2 surface had dimensions of 3.47×3.42 nm^2. The Q_3 surface was prepared similarly by cleaving the $(10\bar{1})$ plane of α-cristobalite and attaching one OH group to each exposed silicon atom. A supercell consisting of $7 \times 4 \times 2$ unit cells of cristobalite was used to prepare the Q_3 surface. It had dimensions of 3.34×3.48 nm^2. For preparing the Q_4 surface, we mimicked the dehydration reaction on the Q_3 surface by deleting one hydrogen atom and one hydroxyl group from adjacent silanol groups and forming a siloxane Si–O–Si bridge between them. This was followed by energy minimization. A snapshot of the three silica surfaces is shown in Fig. 2.

Crude oil is a complex mixture of numerous hydrocarbon molecules of varied molecular weight, and the exact chemical structure of most of the molecules is unknown. The composition and chemistry of these hydrocarbon molecules depend strongly on the geological sources and reservoir conditions. The EOR stage of oil recovery deals with much heavier crude oil fractions, such as asphaltenes, whose precipitation has many implications in the EOR process. Asphaltenes are defined as class of molecules that
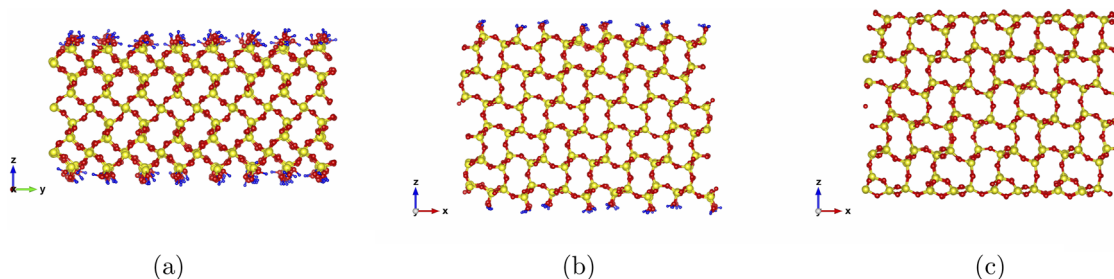
FIG. 2. Side view of the silica slabs with (a) Q_2, (b) Q_3, and (c) Q_4 surfaces used in the simulations. The color coding is as follows: Si (yellow), O (red), and H (blue).

are insoluble in alkanes with short chain lengths, such as pentane or heptane, and soluble in aromatics, such as toluene.[46–48] For this study, we concentrate on the aliphatic portion and use n-heptane as the model aliphatic fluid since it has been used as a representative for the light alkanes in a number of molecular dynamics studies.[49–56] The interactions of n-heptane are described by the TRaPPE force field.[57] Liquid water was modeled by the extended simple point charge model (SPC/E) force field.[58] The cross-interactions for the Lennard-Jones potential were obtained by applying the Lorentz–Berthelot mixing rule. All the Lennard-Jones interactions are truncated and shifted at a cutoff radius of 1.2 nm.

IV. RESULTS

In this work, the contact angles of heptane–water–silica system were computed at a temperature of 318 K. At this temperature, the equilibrium vapor pressure for the heptane–water system was estimated to be 0.124 bar. Since the pressures prevalent in a typical oil reservoir are very high, our simulations were performed at a pressure of 145 bars.

A. Liquid–liquid interfacial free energy

The value of $\gamma^{(ow)}$ was computed using the method of Kirkwood and Buff[21] from simulations of a two phase system consisting of 1449 molecules of water and 159 molecules of n-heptane. The interface had dimensions of 3×3 nm^2 and the length of the simulation box perpendicular to the interface was 10 nm. Periodic boundary conditions were applied in all three directions. The system was equilibrated for 2 ns followed by a production period of 3 ns with a time step of 1 fs. The liquid–liquid interfacial free energy is computed as per Eq. (2) over a series of temperatures varying from 295 to 355 K. The temperature was maintained using a Nosé–Hoover thermostat with a damping parameter of 0.1 ps and the pressure was set to 145 bars using a Nosé–Hoover barostat with a damping constant of 1 ps. The value of $\gamma^{(ow)}$ at 318 K was estimated at 47.5 ± 3 mN/m. The values of $\gamma^{(ow)}$ computed from simulations are compared with experimentally measured values given in Ref. 59 and shown in Fig. 3. On an average, the difference between experimental and simulation data is between 5 and 8 mN/m. We also computed γ for the water–hexane interface for additional force field validation. Our results matched the previously computed results published in Xue et al.[60] and were within 5 mN/m of experimental data.[61]

B. Solid–liquid interfacial free energy

Although one has considerable freedom to choose a cleaving wall potential, we found the following form to be most convenient while using the LAMMPS molecular dynamics package.[42] Similar to Ref. 30, the cleaving wall potential consisted of N_w atoms that only interact with atoms of the liquid. The interaction consists of a combination of repulsive and attractive Born potential and is defined as follows:[62]

$$u_{\text{born}}(r) = A\, e^{-\frac{r-\lambda}{B}} - C\, e^{-\frac{r-\lambda}{D}}, \tag{8}$$

$$u_w(r) = \begin{cases} u_{\text{born}}(r) - u_{\text{born}}(r_c) & \text{if } r < r_c, \\ 0, & \text{otherwise,} \end{cases} \tag{9}$$

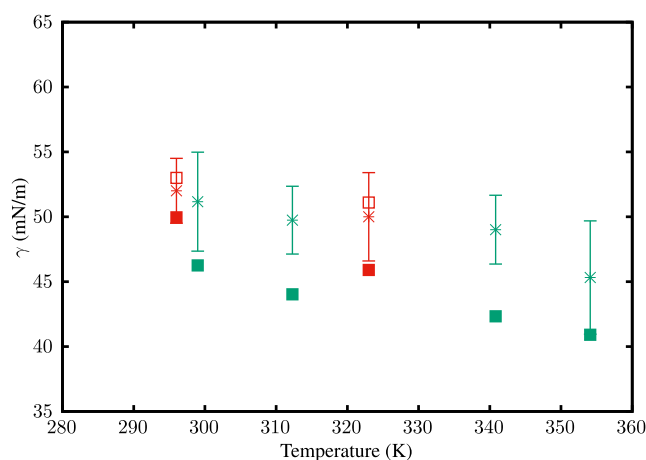$$U_w = \sum_{i=1}^{N_W} \sum_{j=1}^{N_B} u_w(r_{ij}), \tag{10}$$

FIG. 3. Comparison of computed and experimental values of $\gamma^{(ow)}$ at different temperatures for heptane–water (green symbols) and hexane–water systems (red symbols). The filled squares are experimental data from Ref. 59 (heptane) and Ref. 61 (hexane). The empty square corresponds to simulation data for hexane from Ref. 60 and the stars are values computed from our simulations.
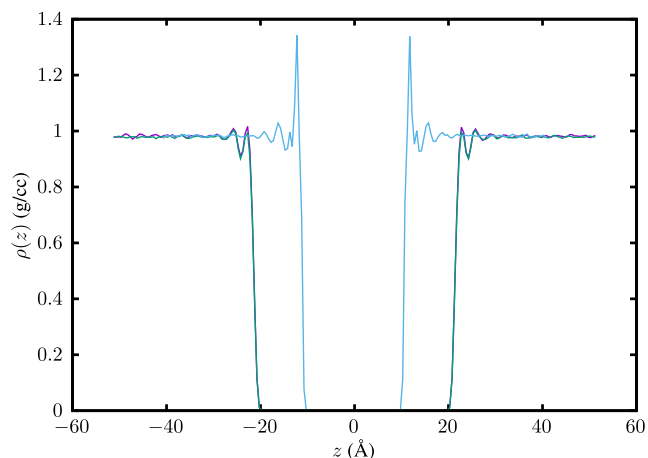
FIG. 4. Density profile of water near the Q_2 surface of silica. The blue line is the density profile of water in contact with the silica surface. The green line is the density profile after cleaving of the liquid water with $\lambda_{max} = 22$ and the purple line is the density profile of the cleaved water with silica slab inserted in the cleaved space.

where N_B is the number of liquid atoms and r_{ij} is the distance between atoms i and j. The values of the constants A, B, C, D were set to 1.0 kcal/mol, 1 Å, 1.05 kcal/mol, 1.4 Å, respectively, and the value of the cutoff distance, r_c, was set to 35 Å. A total of $N_w = 16$ atoms were arranged in a rectangular lattice and placed in a plane perpendicular to the direction in which the liquid is to be cleaved. We used 1200 molecules of water and 400 molecules of n-heptane for simulations of the silica–water and silica–heptane system, respectively.

As mentioned earlier, to ensure the reversibility during the creation of the solid–liquid interface, there has to be minimal change in the structure of the liquid layers near the interface. In order to check whether the value of the constants in Eq. (8) were adequate, we computed the density profile of the liquid phase in these simulations.

In Fig. 4, a plot of the density profile before and after the cleaving of the liquid is shown for both water and heptane near the Q_2 surface. As one can observe, liquid water forms layers when in contact with the silica solid and this layering is also present at the highest value of λ. The simulations for calculation of ΔG_1, ΔG_2, and ΔG_3 consisted of an equilibration stage of 2 ns and a production stage of 2 ns. The temperature was set to 318 K using a Nosé–Hoover thermostat with a damping parameter of 0.1 ps and the pressure was maintained at 145 bars using a Nosé–Hoover barostat with a damping constant of 1 ps. The center of mass of the silica solid was tethered to its initial position via a harmonic spring with a strength of 20 000 (kcal/mol)/Å². The values of λ_{min} and λ_{max} in Eqs. (5) and (6) were set to −6 and 22, respectively, for the Q_2 surface and −6 and 25, respectively, for the Q_3/Q_4 surface. The variation of the integrand for all the three surfaces is given in the supplementary material. The integration for the computation of ΔG_1 and ΔG_3 was carried out using trapezoidal rule. For the calculation of ΔG_2, we generated ten configurations for the solid slab and 10 000 configurations of the liquid phase, giving us a total of 10 × 10 000 terms in Eq. (7). The values of ΔG_1, ΔG_2, and ΔG_3 computed from these simulations are shown in Table I. The table also shows the corresponding values of the contact angles for all the three surfaces. We observe that at the conditions studied, the Q_2 and Q_3 surfaces are completely wetted by liquid water. The computed contact angle for the Q_4 surface is 128° ±5.1°, indicating that it is partially non-wetted by liquid water. These results are along expected lines since the Q_2 surface is the most hydrophilic and the Q_4 surface is the most hydrophobic.

We also examined the structure of the water layer near all the three silica surfaces. To this end, we computed the distribution of the O–O–O angles where the two oxygen atoms were within 4 Å of the central oxygen atom. This distribution was calculated for oxygen atom within a proximity of 5 Å to the silica surface. The computed distributions are shown in Fig. 5 and also compared with the distribution seen in bulk water. We observe that the distribution for Q_2 and Q_3 surfaces is very similar to that for bulk water, indicating that these surfaces are hydrophilic. The distribution near the Q_4 surface differs most from that of bulk water and is a reflection of the hydrophobic nature of this surface.

TABLE I. Changes in the free energy per unit area for each of the steps in the cleaving wall method and corresponding contact angle computed for the water–heptane–silica system. All the values have units of mN/m. The numbers in the parenthesis correspond to uncertainty at 95% confidence interval. The value of $\gamma^{(ow)}$ used to compute θ is 47.5 mN/m. Contact angle of Q_4 surface from direct simulation was 133° ± 11°.

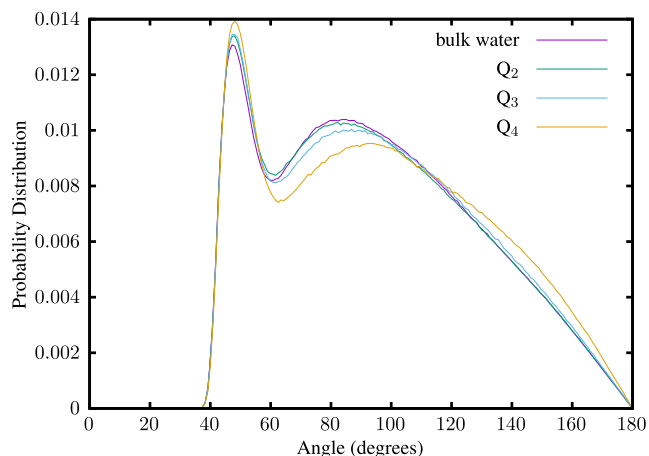|	Q_2 surface		Q_3 surface		Q_4 surface	
	Water	Heptane	Water	Heptane	Water	Heptane
$\Delta G_1/A$	15(1)	−2.2(3)	13(1)	−3.1(4)	13(1)	−3.1(4)
$\Delta G_2/A$	−0.020(4)	−0.022(6)	−0.047(5)	−0.0210(9)	−0.065(4)	−0.0040(4)
$\Delta G_3/A$	−74(1)	−0.8(2)	−54(3)	9(3)	21.4(2)	8(2)
$\gamma^{(os)} - \gamma^{(ow)}$	56(2)		48(3)		−29(2)	
$\cos\theta$	1.2(1)		1.0(1)		−0.62(6)	
θ (deg)	<0		<0		128(5)	

FIG. 5. O–O–O angle distribution for water molecules located within 5 Å of the silica–water interface.

C. Direct simulations of contact angle

Since experimental values of the contact angle for the system being studied were not available for comparison, we performed simulations for direct estimation of the contact angle. The simulations consisted of a cylindrical drop of water immersed in liquid n-heptane and placed on the Q_3 and Q_4 surfaces of silica. The system consisted of 2000 molecules of water and 2400 molecules of n-heptane. The dimensions of the silica slab were 23.35 × 3.48 × 2.194 nm^3. The water molecules were initially arranged in a half cylindrical droplet because cylindrical geometry eliminates the influence of the three phase line tension, which can significantly influence contact angle results at small length scales. The temperature was set to 318 K using a Nosé–Hoover thermostat with a damping parameter of 0.1 ps. The pressure of the system was controlled by piston made up of 912 atoms. The piston atoms interacted with water and heptane by Weeks-Chandler-Andersen (WCA) potential and force is applied on the piston to maintain a system pressure of 145 bars. Periodic boundary conditions were applied in all three directions. The system was equilibrated for 6 ns followed by a production period of 4 ns with a time step of 2 fs. We generated 100 configurations of the system during the production run for analysis of contact angle.
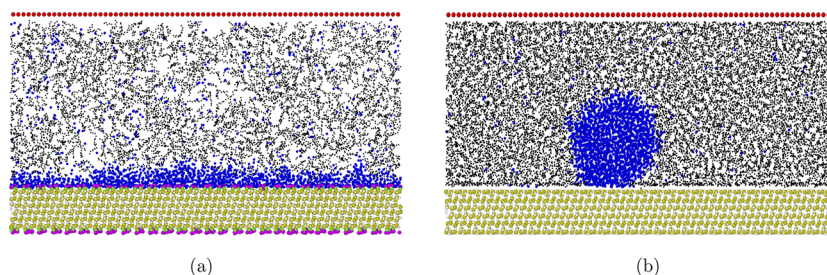
The contact angle was calculated by averaging the two estimates given by the following equations, where h is the height of the droplet, b is the base radius, and r is the droplet radius:

$$\theta = \pi - \arcsin\left(\frac{b}{r}\right), \tag{11}$$

$$\theta = \pi - \arccos\left(\frac{h - r}{r}\right). \tag{12}$$

A snapshot of the system is shown in Fig. 6. From our simulations, we observed that the water droplet completely wetted the Q_3 surface and partially wetted the Q_4 surface. These results are in agreement with the computations using thermodynamic integration. The contact angle computed from the shape of the cylindrical water drop for the Q_4 surface was $133° \pm 11°$, which is close to the value of $128°$ computed using thermodynamic integration.

We now compare and discuss the computational expenses of these two methods. The droplet technique is quite straightforward to implement and the result can be obtained in a single simulation on a large system, while the cleaving wall technique requires a series of simulations on much smaller systems. For the system that was studied in this work, the computational expense of the cleaving wall method is nearly twice that of the droplet method for the same level of statistical uncertainty. In enhanced oil recovery, the liquid water will contain various salts and additives in small concentrations. Under such conditions, one would have to simulate much larger droplets to avoid system-size effects, which will substantially increase the computational expense of the direct method. If estimates of the water contact angle are required in the presence of different liquids, the two methods become competitive since this would only require additional simulations of those liquids, whereas separate simulations have to be performed for each water–liquid combination.

D. Effect of cutoff length

In the results presented until now, we have used a cutoff radius of 1.2 nm for the Lennard-Jones potential. It is well known that the value of the cutoff radius has a strong effect on interfacial properties. To quantify the effect of the cutoff radius, we computed the contact angle with cutoff values varying from 1.0 to 1.3 nm. The method for estimating the contact angles at different values of the cutoff radius is

(a)

(b)

FIG. 6. Snapshots of a water droplet immersed in n-heptane and placed on top of (a) Q_3 and (b) Q_4 surfaces of silica. The blue color represents oxygen atoms of water, the gold color represents silicon atoms of silica, the silver color represents the oxygen atoms of silica, and the red circles at the top represent the piston atoms. The atoms of n-heptane are represented by black dots.

as follows. We start from the definition of the solid–fluid interfacial free energy,

$$\gamma^{(sl)} = \frac{G - G^{(l)} - G^{(s)}}{A}, \qquad (13)$$

where the superscripts (l) and (s) represent the liquid and solid phases, respectively. The change in the value of γ can be obtained by calculating the changes in the values of G, $G^{(l)}$, and $G^{(s)}$. We use the thermodynamic perturbation method to compute the change in free energy, i.e.,

$$G(r_{c_1}) - G(r_{c_2}) = -k_B T \ln\langle e^{-\beta\Delta U}\rangle, \qquad (14)$$

where r_c is the cutoff radius. Accordingly, we have performed simulations of silica–water, silica–heptane, bulk water, and bulk heptane at varying values of the cutoff radius. Since we only need the relative difference in the solid–fluid interfacial free energy, changes in the free energy of the bulk solid were not computed. The changes in the free energy were computed in both the directions, i.e., with increasing and decreasing values of r_c. The two sets of values gave identical results within the precision of our calculation, thus, confirming the accuracy of our estimates. The values of the liquid–liquid interfacial free energy values for varying values of r_c were computed using the Kirkwood–Buff technique. These simulations were performed for the Q_4 surface and the values of the estimated contact angle are shown in Table II. The estimated values of the contact angle were found to be similar within the precision of our calculation. We, hence, conclude that changing the force field cutoff radius for this range of values has a negligible effect on the contact angle.

E. Role of n-heptane

The system considered in this work consists of two fluids, namely, water and n-heptane. Typical measurements of contact angle in laboratories under ambient conditions are for a liquid drop on a surface exposed to air. Although the motivation for our calculations is computation of contact angle under reservoir conditions, it is worthwhile to examine the effect of the second fluid, i.e., n-heptane on the value of the contact angle. The value of the surface tension of water at 318 K was estimated to be 53.16 mN/m. The water–silica interfacial free energies were assumed to be negligibly dependent on pressure and, hence, their values were taken to be the same from the above computations at 145 bars. The air–silica interfacial free

TABLE II. Variation of the interfacial free energies and the contact angles with changes in the force field cutoff radius, r_c. The numbers in the parenthesis correspond to uncertainty at 95% confidence interval.

r_c (nm)	$\gamma^{(so)}$	$\gamma^{(sw)}$	$\gamma^{(ow)}$	$\cos\theta$	θ (deg)
1.00	6(2)	35(1)	50(4)	−0.57(6)	124(6)
1.05	6(2)	35(1)	52(5)	−0.56(7)	124(7)
1.10	6(2)	35(1)	48(3)	−0.60(6)	127(5)
1.15	5(1)	34(1)	51(5)	−0.57(6)	125(6)
1.20	5(1)	34(1)	48(3)	−0.62(6)	128(5)
1.25	4(1)	34(1)	50(3)	−0.58(5)	126(5)
1.30	4(2)	33(1)	51(4)	−0.57(6)	125(6)

energy was assumed to be negligible. With these assumptions, the estimated contact angle for water was 38.9° and 130.2° for the Q_3 and Q_4 surfaces, respectively. For the Q_4 surface, the presence of n-heptane causes only a small change in the value of the contact angle. For the Q_3 surface, there is a big change in the value of the contact angle with the surface now only partially wetted by water. This is because the hydrophilic nature of the surface leads to a higher interfacial free energy for n-heptane compared to air. For the Q_2 surface, the calculations show that the surface will still be completely wetted by water.

V. SUMMARY AND CONCLUSIONS

Using fully atomistic models for all three phases, we have computed the solid–fluid interfacial free energies for water–silica and heptane–silica surfaces and the contact angles for heptane–water–silica and air–water–silica contact systems. Three types of water–silica and heptane–silica surfaces were studied, namely, Q_2, Q_3, and Q_4, which differ in the surface density of terminal silanol groups. The Q_2 and Q_3 surfaces have terminal silanol groups, which make them hydrophilic. We confirmed the same by examining the structure of the water near these surfaces and found them to be similar to that of bulk water. The Q_2 surface has the highest density of silanol groups, and our estimate of the contact angles for both heptane–water–silica and air–water–silica systems showed that the surface is water wet. The Q_3 surface has half the surface density of silanol groups compared to those of the Q_2 surface. Our calculations showed that the surface of this heptane–water–silica system is also completely water wet. However, when air replaced heptane, the water contact angle became greater than 0, i.e., the surface was only partially water wet. The calculations on the Q_4 surface, which has zero terminal silanol groups and is the most hydrophobic, showed that it is partially non-wetted by water. Unlike the Q_3 surface, the value of the contact angles for the heptane–water–silica and air–water–silica systems were nearly the same. These results indicated that the effect of a second fluid, i.e., heptane in this study, on the contact angle is subtle and nonintuitive. We also determined the contact angles using the direct estimation method for the Q_3 and Q_4 surfaces, and the results from both methods were in agreement. Interfacial properties are typically quite sensitive to force field parameters, such as cutoff radius. Hence, we also computed values of the interfacial free energies and contact angles for a range of cutoff values. Within the ranges of the values of the cutoff length, i.e., between 1 and 1.3 nm, the changes in the values of the interfacial properties were negligible.

The thermodynamic Young's equation route of computing the contact angle for the heptane–water–silica system has many advantages over the direct estimation methods. Despite this, the number of studies that use Young's equation is very less when compared to those using the direct estimation method. The main reason for this state of affairs is because the existing implementations of the Young's equation route need the researcher to develop in-house *a la carte* codes, which are not trivial to implement. We demonstrate that contact angle computation using Young's equation, especially for systems involving fluid phases comprised of complex molecules and solid surfaces with detailed surface chemistries, can be performed using LAMMPS without any in-house code modification.

SUPPLEMENTARY MATERIAL

See the supplementary material for variation of the integrands in Eqs. (5) and (6) used to compute ΔG_1 and ΔG_3.

AUTHOR DECLARATIONS

Conflict of Interest

The authors have no conflicts to disclose.

Author Contributions

Rohan Patel: Conceptualization (equal); Data curation (equal); Formal analysis (equal); Funding acquisition (equal); Methodology (equal); Project administration (equal); Resources (equal); Supervision (equal); Writing – original draft (equal); Writing – review & editing (equal). **Ravi Kumar Reddy Addula**: Methodology (equal); Supervision (equal). **Majeed Shaik**: Conceptualization (equal); Data curation (equal); Formal analysis (equal); Project administration (equal); Writing – original draft (equal); Writing – review & editing (equal). **Sudeep N. Punnathanam**: Conceptualization (equal); Funding acquisition (equal); Methodology (equal); Project administration (equal); Resources (equal); Supervision (equal); Writing – review & editing (equal).

DATA AVAILABILITY

The data that support the findings of this study are available from the corresponding author upon reasonable request.

REFERENCES

[1] Statistical review of world energy 2021, https://www.bp.com/content/dam/bp/business-sites/en/global/corporate/pdfs/energy-economics/statistical-review/bp-stats-review-2021-full-report.pdf, 2021.

[2] P. Druetta, P. Raffa, and F. Picchioni, Appl. Energy **252**, 113480 (2019).

[3] L. W. Lake, Enhanced Oil Recovery (Prentice-Hall, Englewood Cliffs, 1989).

[4] T. Ahmed, Reservoir Engineering Handbook (Gulf Publishing Company, Houston, 2000).

[5] L. P. Dake, Fundamentals of Reservoir Engineering (Elsevier, Amsterdam, The Netherlands, 1978).

[6] A. Satter, G. M. Iqbal, and J. L. Buchwalter, Practical Enhanced Reservoir Engineering (PennWell Books, Tulsa, 2008).

[7] O. R. Wagner and R. O. Leach, Trans. AIME **216**, 65 (1959).

[8] G. Javanbakht, M. Sedghi, W. Welch, and L. Goual, Langmuir **31**, 5812 (2015).

[9] F. Jiménez-Ángeles and A. Firoozabadi, J. Phys. Chem. C **120**, 11910 (2016).

[10] A. Silvestri, E. Ataman, A. Budi, S. L. S. Stipp, J. D. Gale, and P. Raiteri, Langmuir **35**, 16669 (2019).

[11] J. Wu, Å. Ervik, I. Snustad, S. Xiao, A. Brunsvold, J. He, and Z. Zhang, J. Phys. Chem. C **123**, 443 (2019).

[12] E. W.-H. Sun and I. C. Bourg, Langmuir **124**, 25382 (2020).

[13] T. T. B. Le, A. Striolo, and D. R. Cole, J. Phys. Chem. C **124**, 18532 (2020).

[14] R. Solc, M. H. Gerzabek, H. Lischka, and D. Tunega, Geoderma **169**, 47 (2011).

[15] D. Argyris, T. Ho, D. R. Cole, and A. Striolo, J. Phys. Chem. C **115**, 2038 (2011).

[16] F. Taherian, V. Marcon, N. F. A. van der Vegt, and F. Leroy, Langmuir **29**, 1457 (2014).

[17] N. Wei, C. Lv, and Z. Xu, Langmuir **30**, 3572 (2014).

[18] J. Zhao, G. Yao, and D. Wen, Fuel **272**, 117615 (2020).

[19] H. Jiang, F. Müller-Plathe, and A. Z. Panagiotopoulos, J. Chem. Phys. **147**, 084708 (2017).

[20] H. Jiang and A. J. Patel, Curr. Opin. Chem. Engg. **23**, 130 (2019).

[21] J. G. Kirkwood and F. P. Buff, J. Chem. Phys. **17**, 338 (1949).

[22] J. Q. Broughton and G. H. Gilmer, J. Chem. Phys. **84**, 5759 (1986).

[23] R. L. Davidchack and B. B. Laird, J. Chem. Phys. **118**, 7651 (2003).

[24] J. R. Morris and X. Song, J. Chem. Phys. **119**, 3920 (2003).

[25] E. M. Grzelak and J. R. Errington, J. Chem. Phys. **128**, 014710 (2008).

[26] F. Leroy, D. J. V. A. dos Santos, and F. Müller-Plathe, Macromol. Rapid Commun. **30**, 864 (2009).

[27] R. Benjamin and J. Horbach, J. Chem. Phys. **141**, 044715 (2014).

[28] J. R. Espinosa, C. Vega, and E. Sanz, J. Chem. Phys. **141**, 134709 (2014).

[29] X. Qi, Y. Zhou, and K. A. Fichthorn, J. Chem. Phys. **145**, 194108 (2016).

[30] R. K. R. Addula and S. N. Punnathanam, J. Chem. Phys. **153**, 154504 (2020).

[31] W. Guo and J. R. Errington, J. Phys. Chem. C **122**, 17309 (2018).

[32] W. Guo and J. R. Errington, Langmuir **35**, 6540 (2019).

[33] T. Saito, E. Shoji, M. Kubo, T. Tsukada, G. Kikugawa, and D. Surblys, J. Chem. Phys. **154**, 114703 (2021).

[34] C. Bistafa, D. Surblys, H. Kusudo, and Y. Yamaguchi, J. Chem. Phys. **155**, 064703 (2021).

[35] K. Jain, K. S. Rane, and J. R. Errington, J. Chem. Phys. **150**, 084110 (2019).

[36] K. Jain, A. J. Schultz, and J. R. Errington, J. Chem. Phys. **151**, 044103 (2019).

[37] R. Yan, W. Z. Sun, S. D. Ma, R. L. Davidchack, N. Di Pasquale, Q. J. Zhai, T. Jing, and H. B. Dong, Comput. Mater. Sci. **155**, 136 (2018).

[38] R. L. Davidchack and B. B. Laird, J. Chem. Phys. **108**, 9452 (1998).

[39] R. L. Davidchack and B. B. Laird, Phys. Rev. Lett. **85**, 4751 (2000).

[40] R. Handel, R. L. Davidchack, J. Anwar, and A. Brukhno, Phys. Rev. Lett. **100**, 036104 (2008).

[41] R. L. Davidchack, R. Handel, J. Anwar, and A. V. Brukhno, J. Chem. Theory Comput. **8**, 2383 (2012).

[42] S. Plimpton, J. Comput. Phys. **117**, 1 (1995).

[43] M. J. Abraham, T. Murtola, R. Schulz, S. Páll, J. C. Smith, B. Hess, and E. Lindahl, SoftwareX **1**, 19 (2015).

[44] J. C. Phillips, R. Braun, W. Wang, J. Gumbart, E. Tajkhorshid, E. Villa, C. Chipot, R. D. Skeel, L. Kalé, and K. Schulten, J. Comput. Chem. **26**, 1781 (2005).

[45] F. S. Emami, V. Puddu, R. J. Berry, V. Varshney, S. V. Patwardhan, C. C. Perry, and H. Heinz, Chem. Mater. **26**, 2647 (2014).

[46] J. G. Speight, R. B. Long, and T. D. Trowbridge, Fuel **63**, 616 (1984).

[47] Structures and Dynamics of Asphaltenes, edited by O. C. Mullins and E. Y. Sheu (Springer Science+Business Media, LLC, 1995).

[48] H. W. Yarranton, H. Alboudwarej, and R. Jakher, Ind. Eng. Chem. Res. **39**, 2916 (2000).

[49] A. Ortega-Rodríguez, S. A. Cruz, A. Gil-Villegas, F. Guevara-Rodríguez, and C. Lira-Galeana, Energy Fuels **17**, 1100 (2003).

[50] A. N. M. Carauta, P. R. Seidl, E. C. A. N. Chrisman, J. C. G. Correia, P. d. O. Menechini, D. M. Silva, K. Z. Leal, S. M. C. de Menezes, W. F. de Souza, and M. A. G. Teixeira, Energy Fuels **19**, 1245 (2005).

[51] T. Kuznicki, J. H. Masliyah, and S. Bhattacharjee, Energy Fuels **22**, 2379 (2008).

[52] T. F. Headen, E. S. Boek, and N. T. Skipper, Energy Fuels **23**, 1220 (2009).

[53] I. A. Wiehe, Energy Fuels **26**, 4004 (2012).

[54] M. Sedghi, L. Goual, W. Welch, and J. Kubelka, J. Phys. Chem. B **117**, 5765 (2013).

[55] C. Jian, T. Tang, and S. Bhattacharjee, Energy Fuels **28**, 3604 (2014).

[56] L. Ramírez, I. Moncayo-Riascos, F. B. Cortés, C. A. Franco, and R. Ribadeneira, Energy Fuels **35**, 3119 (2021).

[57] M. G. Martin and J. I. Siepmann, J. Phys. Chem. B **102**, 2569 (1998).

[58] H. J. C. Berendsen, J. R. Grigera, and T. P. Straatsma, J. Phys. Chem. **91**, 6269 (1987).

[59] S. Zhang, X. Lu, J. Wu, W. Tong, Q. Lei, and W. Fang, J. Chem. Eng. Data **59**, 860 (2014).

[60] B. Xue, D. B. Harwood, J. L. Chen, and J. I. Siepmann, J. Chem. Eng. Data **63**, 4256 (2018).

[61] G. Wiegand and E. U. Franck, Ber. Bunsengesellschaft Phys. Chem. **98**, 809 (1994).

[62] In order to implement the wall interaction using LAMMPS without modifying it, each site for the wall is split into two: one for repulsive and the other for attractive interaction, respectively.